Soft Matter

Contact criterion for suspensions of smooth and rough colloids

Journal:	*Soft Matter*
Manuscript ID	SM-ART-01-2020-000072.R1
Article Type:	Paper
Date Submitted by the Author:	26-Mar-2020
Complete List of Authors:	Pradeep, Shravan; North Carolina State University, Chemical and Biomolecular Engineering Hsiao, Lilian; North Carolina State University, Chemical and Biomolecular Engineering

Contact criterion for suspensions of smooth and rough colloids

Shravan Pradeep & Lilian C. Hsiao*

Department of Chemical and Biomolecular Engineering, North Carolina State University, Raleigh, NC 27695, USA

*Corresponding author.

Email: lilian_hsiao@ncsu.edu

ABSTRACT

We report a procedure to obtain the search distance used to determine particle contact in dense suspensions of smooth and rough colloids. This method works by summing physically relevant length scales in an uncertainty analysis and does not require detailed quantification of the surface roughness. We suspend sterically stabilized, fluorescent poly(methyl methacrylate) colloids suspended in a refractive index-matched solvent, squalene, in order to ensure hard sphere-like behavior. High speed centrifugation is used to pack smooth and rough colloids to their respective jamming points, ϕ_J. The jammed suspensions are subsequently diluted with known volumes of solvent to $\phi < \phi_J$. Structural parameters obtained from confocal laser scanning micrographs of the diluted colloidal suspensions are extrapolated to ϕ_J determine the mean contact number at jamming, $\langle z \rangle_J$. Contact below jamming refers to a length scale below which the effects of hydrodynamic or geometric friction come into play. Sensitivity analyses show that a deviation of the search distance by 1% of the particle diameter results in $\langle z \rangle$ changing by up to 10%, with the error in contact number distribution being magnified in dense suspensions ($\phi > 0.50$) due to an increased number of nearest neighbors in the first coordination shell.

1. Introduction

Grains, colloids, foams, and emulsions belong to a class of particulate suspensions found in many scientific and technological applications, ranging from geophysical phenomena to consumer goods. The mechanical load-bearing properties of these materials become significant when the constituent particles are densely packed together in the absence of attractive interactions. As more and more particles are added to the suspension, each particle experiences a caging effect from its nearest neighbors, along with hydrodynamic effects from the suspending fluid. The entire material jams when the particle volume fraction ϕ increases to a point near random close packing (RCP): it transitions from a free-flowing state to a rigid state with an effectively infinite zero-shear viscosity.[1, 2] The nature of this transition depends on a number of material parameters such as thermal fluctuations, particle deformability, the softness of the interaction potential, and the shape and morphology of the particles. Jamming is widely observed in biological and engineered systems: diseased cells tend to jam more readily than their healthy counterparts[3], flocks of sheep jam when herded through gates[4], and grains discharging from silos may become "stuck".[5]

Seminal work by Liu and Nagel[6], as well as by O'Hern and coworkers[7], established a jamming state diagram for particulate matter based on temperature, load, and density. The mean contact number $<z>$, the average number of contacting neighbors for a particle, was identified as a crucial microscopic parameter that is intimately coupled to the jamming point of athermal suspensions in which hydrodynamic contributions from the continuum are small. The rationale is that contacts between particles generate force chains that sum up to the overall stress in a material.[8-12] When the force chains become space-spanning and zero floppy modes of deformation remain, the particulate material becomes mechanically rigid at the isostatic

condition, where the contact number is z_{iso} = 6 for frictionless spheres.[2] Follow-on experiments and simulations have since confirmed the strong connection between $\langle z \rangle$ and the bulk modulus of various materials with and without interparticle attraction. The viscoelasticity of attractive colloidal gels is attributed to the contact number distribution within strands that contain particles at volume fractions ϕ near random close packing (ϕ_{RCP}), which in turn affects their structural and dynamical evolution.[13-18] Simulations of soft repulsive spheres interacting through Hertzian contacts and an interparticle friction μ_p show that the shear modulus scaled with bulk modulus or material stiffness exhibits a linear power-law scaling with respect to the excess contact number, $\Delta z = \langle z \rangle - z_{iso}$.[19-22] When prolate and oblate spheroids of different aspect ratios are used, ϕ_{RCP} increases, with a corresponding increase in $\langle z \rangle$ at RCP.[23, 24] More recently, the deformable particle model enables arbitrary particle shapes to be described by an energy function that captures the onset of jamming for 2D deformable polygons.[25] Experimental approaches have utilized granocentric models to capture the jammed microstructure of polydisperse emulsion packings.[26, 27] Importantly, the correlation between mechanics and contact microstructure scales as the distance to jamming $\langle z \rangle - z_J$ and $\phi - \phi_J$, where the subscript J refers to the jamming point. This correlation uses the excess parameters instead of the absolute value of ϕ or $\langle z \rangle$, because z_J and ϕ_J change depending on particle properties and how the packing is generated. As an example, the scaling behavior of properties such as elastic modulus, external osmotic pressure, and low-frequency modulus had been correlated with the distance from the RCP structure in compressed emulsions.[28, 29] The idea of scaling with the distance to jamming is widely accepted in the granular matter literature but has not yet been experimentally validated in the field of colloidal suspensions.

The key difference between the two types of particulates is that colloidal suspensions exhibit thermal fluctuations over experimental time scales, while granular media are athermal in nature. The diffusive motion of the colloids generates a hydrodynamic resistance that contributes to the suspension stress in dilute conditions.[30] As ϕ increases beyond ≈ 0.50, calculations of suspension stress based solely on near- and far-field hydrodynamics begin to perform poorly[31, 32], likely because the contact stresses between particles become more granular-like.[33] However, unlike the case of athermal grains where a pile will not support any stress unless it is at $\phi \geq \phi_{RLP}$, where RLP is the random loose packing state,[34] stochastic Brownian fluctuations in colloidal suspensions give rise to transient clusters that support a finite viscoelasticity below ϕ_{RCP}. The viscoelasticity and rheology of the hard-sphere colloidal suspensions close to RCP is very well established.[35-37] Experimentally, a connection between colloidal and granular shear thickening was made using hard sphere particles of moderate sizes ($1\ \mu m \leq 2a \leq 50\ \mu m$).[38] Additionally, particles with surface asperities possess greater interparticle friction than their smooth counterparts[39, 40] and this results in flow with greater hydrodynamic and contact resistance under applied stress, especially at higher ϕ.[33, 41] Soft particles, such as microgels[42-44] and colloidal star polymers,[45] do not jam unless packed to much higher volume fractions ($\phi_J \to 1$) because of their ability to deform or interpenetrate. Just as in the case of hard spheres, their dynamical arrest and rheological properties are highly dependent on the distance of ϕ from ϕ_J.

A number of experimental challenges persist in obtaining a physically accurate value of $\langle z \rangle$ even with hard sphere-like colloids. Conventionally, the contact distance is approximated as the primary minimum in the radial distribution function, $g(r)$.[46] This is done to account for uncertainties in the average particle-to-particle separation distance, which come from a few sources: (a) sterically-stabilized particles tend to have surface-grafted polymer brushes, which

can adopt different conformations depending on the grafting density and the polymer-solvent interactions[47] (**Fig. 1**), (b) incomplete screening of the electrostatic repulsion gives rise to a finite Debye screening length, and (c) most particles are polydisperse in size and surface roughness. The effect of the contact distance in characterizing load-bearing colloidal packings has been previously discussed in literature.[48, 49] Due to the importance of contact microstructure in particulate micromechanics, setting a contact criterion to establish an accurate value of $\langle z \rangle$ near jamming is critical. Some of the earlier works to establish a contact criterion in experimental systems include the use of black japan paint marks for packing of ball bearings[50] and interfacial fluorescent dyes in an emulsion system.[51] These methods tend to be time consuming and possess challenging surface chemistry modification in the case of experimental hard sphere colloids, which are used as model systems for studying colloidal phase behavior and rheology.

We report a method to extract the contact criterion from microscopy images of hard sphere-like smooth and rough colloids suspended in a refractive index-matched solvent at $\phi >$ 0.10. The poly(methyl methacrylate) (PMMA) colloids are fluorescent and sterically stabilized with a grafted layer of poly(12-hydroxystearic acid) (PHSA).[52, 53] They are packed to a jammed state, ϕ_J, by high speed centrifugation, then diluted subsequently and imaged with a confocal laser scanning microscope (CLSM). The resultant suspension microstructures are compared to liquid state theory. Finally, we obtain the contact search distance by considering the physical length scales between two neighboring particles and comparing our results with the simulation data of Silbert for particles with varying pairwise friction coefficient, μ_p.[54]

2. Materials and Methods

2.1 Synthesis and characterization of PHSA comb copolymer as the steric stabilizer

All chemicals were purchased from Sigma-Aldrich and used without further purification unless specified. Smooth and rough colloids were synthesized *via* free-radical dispersion polymerization using the PHSA comb copolymer stabilizer synthesized in our lab. The PHSA stabilizer was synthesized using a standard three-step synthesis process[52] (**Fig. 2a**): first, the polycondensation of 12-hydroxystearic acid (12-HSA, 80% purity from TCI Chemicals) into PHSA in the solvent toluene, using the catalyst p-toluenesulfonic acid at temperature of 150˚C over a period of 20-22 hours; second, the synthesis of PHSA-glycidyl methacrylate (PHSA-GMA) brushes in toluene at 150˚C for 7 hours; finally, the free-radical polymerization of PHSA-GMA using the heat-activated initiator 2-azobisisobutyronitrile (AIBN) and the monomer methyl methacrylate (MMA) in a 2:1 wt % mixture of ethyl acetate and butyl acetate at 110˚C for 9.5 hours to produce PHS-GMA-MMA block copolymer brushes. Both GMA and MMA were used after removing the trace amount of stabilizing inhibitors by passing them through an inhibitor removal column, purchased from Sigma-Aldrich. The average number of monomer per chain of the PHSA-GMA brushes was characterized using nuclear magnetic resonance (NMR) spectroscopy (Bruker NEO 400 MHz). Deuterated chloroform ($CDCl_3$) was used as the solvent for the NMR measurements.

The length of the brush chain on the particles is linearly related to the number of monomer units per chain (n) in the PHSA-GMA intermediate from PHSA stabilizer synthesis. Here, we utilized two methods to characterize the value of n. First, we performed ^{1}H-NMR on the monomer 12-HSA and the intermediate product PHSA-GMA. The intensity spectra was normalized by the background solvent intensity ($CDCl_3$). This method utilizes the change in peak signals for corresponding chemical shifts (δ) of the respective proton. In our case, these are hydrogen atoms in the unreacted carbon atom ($\delta \sim 3.6$ ppm) and the newly formed ester ($\delta \sim 4.8$

ppm) in the 12-HSA and PHSA-GMA. As the polycondensation reaction proceeds, the former peak decreases while the later peak increases, as shown in **Fig. 2b.** The average number of monomer units per chain ($\overline{x_n}$) was computed by integration of the peaks corresponding to the ester and alcohol groups using the formula:[53]

$$\overline{x_n} = \frac{1}{\frac{n_{OH}}{r n_{ester}} + \frac{1}{r} - 1} + 1 \quad (1)$$

Here, n_{OH} and n_{ester} correspond to the number of alcohol and ester groups present in the PHSA-GMA adduct. We obtained the ratio n_{ester}/n_{OH} = 10.73 by integrating the intensities at their peaks, and estimated the initial monomer purity, *r*, as 0.8975. Value of *r* for 80% pure 12-HSA used in our synthesis was linearly interpolated from *r*-monomer purity data reported in Palangetic et al. Substituting n_{ester}/n_{OH} and *r* into equation (1) shows that $\overline{x_n}$ = 5.586. To independently verify the number of monomer units per PHSA copolymer chain, we estimated the number of acid groups by titrating the PHSA adduct against 0.01 M potassium hydroxide (KOH) solution, and found that the average number average molecular weight was $\overline{M_n}$ = 1668 g/mol and $\overline{x_n}$ = 5.551. Previous studies reported that a length of 5-6 monomer units in PHSA is equivalent to a stabilizer brush length of 10-15 nm.[55] Unlike the previous work (95% purity)[53], we showed that PHSA stabilizer can be synthesized from a lower grade (80% purity) 12-HSA monomer.

2.2 Synthesis and characterization of smooth and rough colloids

PMMA colloids were synthesized using the PHSA comb copolymer as the steric stabilizer (**Fig. 2c**). For smooth colloids, 1.8 g of PHSA stabilizer was added into a 250 ml three-

necked reaction flask containing 2:1 wt/wt% solvent mixture of hexane and dodecane. The mixture was stirred while increasing the temperature to 80˚C to maintain reflux. Then, a mixture of 0.2775 g AIBN, 34 g MMA, 230 µl 1-octanethiol, and 660 µl methacrylic acid was added to the flask. Nucleation commenced four to eight minutes after the addition of the monomer solution, determined as the time at which the clear solution began to turn cloudy. Rough PHSA-*g*-PMMA colloids were synthesized in the same manner as the smooth colloids, but with the addition of the crosslinker ethylene glycol dimethacrylate, EGDM, (EGDM/PHSA = 1.4 wt/wt%) at a rate of 360 µl/min after nucleation commenced. All colloids were fluorescently dyed with Nile Red to allow visualization during CLSM measurements. After two hours of reaction, the reaction flask was cooled to room temperature. Particles formed in the reaction flask were cleaned with pure hexane for a minimum of six times by centrifugation at 10,000 rpm for 15 minutes. The clean particles were stored in hexane until further use. A field emission scanning electron microscope (FEI Verios 460L) was used to image the samples, which were deposited on a silicon substrate and sputter coated with 8-9 nm of Au/Pd. The micrographs in **Fig. 3a** show that the smooth colloids are of particle diameters $2a_{SEM}$ = 1.45 µm ± 4%, while the rough colloids are of effective particle diameters $2a_{eff,SEM}$ = 1.43 µm ± 8%. These particle diameters are reported for dry particles, which undergo swelling when suspended in solvents. Atomic force microscopy (AFM) (Asylum MFP-3D) was used to qualitatively illustrate the difference in surface roughness profiles (**Fig. 3b**) using a silicone cantilever tip (force constant = 5 N/m, resonant frequency = 150 kHz and tip radius < 10 nm) in tapping mode.

2.3 Preparation of colloidal suspensions

Dense colloidal suspensions were prepared by performing a solvent transfer of the PMMA particles into squalene (viscosity η = 12 cP at 25°C). Particles are charge neutral in this solvent and exhibit hard sphere-like behavior. The solvent is refractive index-matched with the particles (refractive index n_{PMMA} = 1.49 and n_{squalene} = 1.49), which reduces scattering in 3D CLSM and minimizes the van der Waals attractions between the colloids. There is a density mismatch of $\Delta\rho$ = 0.322 g/cm^3 between the particles and the solvent (density ρ_{PMMA} = 1.18 g/cm^3 and ρ_{squalene} = 0.858 g/cm^3). The density mismatch was used to generate colloidal suspensions at maximum packing by centrifuging the suspensions at high speeds until the particles completely settled to the bottom of the centrifuge tubes[56]. It should be noted that our protocol shifts the maximum random close packing (ϕ_{RCP}) to a lower shear-jammed value (ϕ_{J}), which is process- and μ_{p}-dependent.[57-59] The Péclet number for sedimentation, $Pe_g = 4\pi a^4\Delta\rho g/3k_BT$, is a dimensionless number that defines the ratio of the sedimentation rate to the rate of Brownian motion. Centrifugation was performed at Pe_g = 1400 to avoid crystallization of the monodisperse colloids.[60] After removal of excess solvent, the compacted samples were diluted from ϕ_{J} by gradual addition of known small volumes of squalene. Diluted suspensions were tumbled in vials at 3 rpm for a minimum of one week to achieve even re-dispersion. For smooth colloids, the volume fraction $\phi_{dilution}$ was computed from the ratio of $\phi_{dilution} = V_p/(V_p+V_s')$, where $V_s' = V_s+V'$. Here, V_P and V_S are the volume of particles and solvent at known ϕ_{J} calculated from mass balance, and V' is the additional volume of solvent added for dilution from ϕ_{J}. This method was used to generate suspensions of smooth and rough colloids with $0.1 \leq \phi \leq \phi_{\mathrm{J}}$.

2.4 CLSM imaging and image processing

A high speed CLSM (Leica SP8) equipped with a resonant scanner was used to visualize the 3D microstructure of smooth and rough colloidal suspensions. The diluted suspensions were transferred to glass vials with an attached coverslip with dimensions of 40 mm × 24 mm and a thickness of 0.21 ± 0.04 mm for imaging. Images were obtained at ≥ 15 μm above the bottom cover slip to avoid wall-induced crystallization effects. The dimensions of the image volume (V_{box}) were 30.72 μm × 30.72 μm × 15 μm, with a voxel size of 0.06 μm × 0.06 μm × 0.06 μm. Imaging was performed at three independent locations within the same sample. Each image volume was captured in 8-10 s, which is much shorter than the Brownian diffusions time scales (τ_B) as defined by the Stokes-Einstein-Sutherland diffusivity ($\tau_B = 6\pi\eta a_{eff}^3/k_BT$; $\tau_{B,smooth} = 29$ s and $\tau_{B,rough} = 20$ s). This ensures that the inherent Brownian motion of these microspheres does not significantly affect centroid identification in image processing. A minimum of 3000 particles per image volume was used to generate sufficient statistics for structural characterization.

Particles positions in 3D were obtained by a standard imaging algorithm in which the brightest weight-corrected pixels correspond to particle centroids.[61] Raw images and corresponding centroid-picked images for smooth and rough particles are shown in **Fig. 4**. The $g(r)$ was obtained by computing the density-normalized probability of finding particles around a reference centroid. The volume fraction was directly obtained from the images using the relation, $\phi_{CLSM} = (4/3)\pi a_{eff}^3 N_p/V_{box}$, where N_p is the total number of particles found in the image volume V_{box}. The value of ϕ_{CLSM} and $\phi_{dilution}$ are in agreement as shown in **Fig. 5a**. The direct imaging method combined with a dilution factor is critical in the estimation of ϕ for rough colloids where ϕ_J is unknown, because of difficulties with sample handling near ϕ_J. This analysis showed that $\phi_J = 0.64$ for the smooth colloids, while $\phi_J = 0.56$ for the rough colloids. For a smooth hard sphere system with 4% size polydispersity, simulations show that the maximum close packing ϕ_{RCP} has

been shown to lie between 0.64 and 0.66.[62-64] Experiments on the effect of particle polydispersity and shape was characterized earlier using higher moments of *2a*, namely skewness and kurtosis, and ϕ_{RCP} was found to be in between 0.63-0.69.[65] Due to the shear-jamming nature of the high Pe_g centrifugation method, both smooth and rough colloids jam below ϕ_{RCP}. In case of smooth PMMA particles, we do not observe a significant shift from simulated/theoretically predicted ϕ_{RCP} despite the soft repulsive nature of the grafted polymers. The contact number distribution p(z) and the mean contact number $\langle z \rangle$ were obtained from microstructural data by averaging the number of particles around a reference centroid as a function of the search distance, $r' = r/2a_{eff}$, where r' ranges from 1 to 1.1.

PMMA colloids swell in certain solvents[66] and in our samples we observe that the particle diameters increase by 1-12% when suspended in squalene. Thus, using the dry particle sizes obtained from SEM results in underestimation of the suspension volume fraction by 28% for smooth particles, and by 4% for rough particles. To obtain the swollen particle diameter of smooth and rough colloids in squalene, we obtained 2D images of the bottom-most monolayer of sediment particles in glass vials, where the z-plane is adjusted to match the centers of most of the particles. Because $\phi \sim a^3$ and therefore $\Delta\phi \sim 3\phi\Delta a$, we paid special attention to the measurement of the effective particle diameter for the rough colloids.[67] In this study, we considered the surface-to-surface distance of rough colloids, which provides a value of $2a_{eff}$ that minimizes the deviation of the surface roughness as shown in **Fig 5b**. The swollen diameters of the smooth and rough colloids were $2a_{smooth} = 1.61$ μm ± 4% and $2a_{eff,rough} = 1.44$ μm ± 5%. The difference in the swelling between smooth and rough colloids are likely due to the presence of crosslinker in the rough microspheres.[66]

3. Results and Discussion

3.1 Radial distribution function

The suspension microstructures of smooth and rough colloids in squalene are quantified in **Fig. 6**. The experimentally measured $g(r)$ of the dense suspensions are plotted alongside predictions from the Ornstein-Zernicke integral equation of state[68]:

$$h(r) = c(r) + \rho \int c(|r - r'|h(r')).dr' \tag{2}$$

Here, $g(r) = h(r)+1$, where $h(r)$ represents the correlation function that takes into account the direct contribution from two-body interactions and the indirect contribution from multi-body interactions. Equation (2) produces an analytical solution for the $g(r)$ when the Percus-Yevick closure for hard spheres is used[69] in which $g(r) = 0$ for $r < 2a$ and $c(r) = 0$ for $r > 2a$:

$$g(r) = 1 + c(r) + \frac{4\pi}{(2\pi)^3} \int_0^1 k^2 \sin(kx) \frac{c(k)}{kx} \left[\frac{\phi \frac{6}{\pi} c(k)}{1 - \phi \frac{6}{\pi} c(k)} \right] dk \tag{3}$$

The excellent agreement between the theoretical and experimental $g(r)$ in **Fig. 6** shows that both smooth and rough colloids exhibit hard sphere-like behavior. Additionally, the absence of regularly spaced, sharp peaks in the $g(r)$ shows that the suspensions remain disordered and non-crystalline in our experimental timescales.

In **Fig. 6**, there is a discrepancy in the first $g(r)$ maxima and minima between the experimental data and theoretical predictions for both smooth and rough colloids when $\phi > 0.50$. We hypothesize that this mismatch is due to the sensitivity of the image processing algorithm to size polydispersity in suspensions at higher concentrations, which has been reported previously in literature for $\phi > 0.26$.[70] Our experimental $g(r)$ are similar to that obtained by Mason and coworkers, who investigated the structure of polydisperse emulsions through experiments and

Brownian Dynamics simulations.[71] To verify that the variation in our case does not undercount N_p and the mean contacts, we apply a similar concept from atomic liquids where the the total number of particles in the first coordination shell, N, is computed using the integral, $\int_0^{\infty} 4\pi r^2 \rho g(r) dr \approx N$ where ρ is the number density of particles. Specifically, N particles fill the volume around the first coordination shell as defined by the primary minimum ($r_{\min}$) of $g(r)$. Since colloids are thought to be "model atoms", N was conventionally used to obtain the mean contact number.[72-75] While the concept of coordination number is useful in describing the structure of dense liquid phase[76], it is not the same as the number of direct particle-particle contacts, which is required to establish the contact criterion required for mechanical stability. Nonetheless, we know that N from both experimental and theoretical $g(r)$ for the same ϕ should match. We use this idea to comment on the accuracy of our experimental $g(r)$. We estimate N by discretizing the above integral as $\sum_{r=0}^{r_{\min}} g(r_i) r_i^2 \Delta r$, where Δr is the binned intervals of the discretized $g(r)$. For a smooth suspension of $\phi = 0.57$, we obtain N as 10.8 and 11.9, from experimental and theoretical *g(r)*, respectively. The small differences may be due to bin-size sensitivity in discretizing the integration and approximation of the integral as $\int_0^{r_{\min}} 4\pi r^2 \rho g(r) dr = N - 1 \approx N$. We conclude that even though our image processing is sensitive to polydispersity at higher ϕ, the algorithm does not undercount N_p in the 3D image volumes.

3.2 Physical rationale of the contact cutoff distance and verification with simulations

We define r' as the additional length scale beyond that of the swollen particle diameter that determines contact between two particles. It is obtained by propagating the uncertainties

introduced by size polydispersity, the length of the PHSA steric layer on particle surfaces, and the average length scale of the asperities present on the rough colloids. We first discuss the results obtained from using this contact criterion on dense suspensions of smooth colloids. The true swollen particle diameter is given as $2a_{true} = 2(a+l)$, where l is the length of PHSA brush. Uncertainty propagation in particle size estimation is given by $\Delta 2a_{true} = [(\Delta 2a)^2+(\Delta l)^2]^{1/2}$. Since $2a$ = 1.62 μm for the smooth colloids, combining the uncertainty from particle polydispersity (± 0.06 μm) and the uncertainty from PHSA brush length measurements from the literature for 5-6 monomer units (± 6 nm) [55, 77-79] yields a total uncertainty of 4%. This method suggests that a value of r' = 1.04 defines contact between smooth colloids. The uncertainty in $2a_{eff}$ for rough colloids includes the added length scale from the surface bumps, which is also inherent in the size polydispersity due to the method with which we obtained particle diameters. The rough colloids have a size polydispersity of ± 0.07 μm. Here, we do not use the roughness length scale or the interparticle friction for this set of particles. As in the case of smooth colloids, addition of the uncertainty from PHSA brush length yields an overall size uncertainty of 5%. This establishes the contact criterion as r' = 1.05 for the rough colloids.

To verify that these values of r' represent the correct contact physics found in dense colloidal suspensions, we first obtain $\langle z \rangle$ of all suspensions generated with different r' values. Then, we extrapolate $\langle z \rangle$ to ϕ_J using and empirical fit and compare the mean contact numner at the shear jammed condition with simulated $\langle z \rangle_J$ values for frictionless and frictional spheres in the absence of solvent hydrodynamics.[54] Mechanical isostaticity, which controls the jammed state at RCP, dictates that $\langle z \rangle_{RCP} = 6$ for smooth or frictionless particles. Our smooth particles can be assumed as frictionless because we showed earlier that the experimentally calculated ϕ_J and the theoretically established ϕ_{RCP} are very close to each other. The concept of isostaticity at

RCP justifies extrapolation of the data for smooth colloids to ϕ_J, where the experimental value of $\langle z \rangle_J$ is expected to be six. The benchmarking against predicted values of $\langle z \rangle_J$ for smooth (frictionless) and rough (frictional) colloids is used to generate an independent validation of the experimental contact criterion r'.

Surface anisotropy in the form of microscale bumps is thought to cause interlocking hindrance, which is a form of geometric friction caused by the inability of rough colloids to rotate freely in the solvent. This concept is supported by our earlier experimental observations that the rotational dynamics of rough colloids was far slower than that predicted by Stokesian Dynamics simulations.[40] We used this idea to determine if the physical rationale behind the value of of r' is correct by comparing the value of $\langle z \rangle_J$ obtained with different r' for smooth and rough colloids with the results from friction-dependent simulations of monodisperse granular spheres. The computer simulations of Silbert[54] probed the packing microstructure and force chains of a 3D packing of inelastic soft spheres that was first quenched by overcompression beyond jamming point, then brought back to the point of isostaticity by expanding the box and allowing $\phi \rightarrow \phi_J$. The protocol was repeated with the addition of a Coulomb friction criterion between spheres. Silbert described two interesting observations: first, the value of ϕ_J decreased from 0.64 to 0.55 when the interparticle friction μ_p increased from 0.001 to 10; second, the distribution of contact stresses depended on μ_p and the history of the packing. Furthermore, the reduction in ϕ_J with the increased frictional constraint between particles was accompanied by a corresponding reduction in $\langle z \rangle_J$ from six to four, which we reproduce in **Fig. 7** for comparison against experimental data. Silbert's simulations showed that the correlation between $\langle z \rangle_J$ and μ_p is nonlinear: at $\mu_p < 10^{-2}$, $\langle z \rangle_J$ remains close to six while at $\mu_p > 1$, $\langle z \rangle_J$ saturates near a value of four. We assume that our smooth colloids behave like frictionless spheres while the rough

colloids in the shear jammed condition behave like frictional spheres. Previous experimental studies have shown that changing the surface roughness of colloids caused changes in μ_p.[33, 39, 80] We did not perform lateral force microscopy to measure the sliding friction between particles, so we do not know the exact value of μ_p for the rough particles used in this study.

3.3 Sensitivity analysis of contact distance criterion

Fig. 8 demonstrates the sensitivity of $\langle z \rangle$ to the choice of r'. For example, arbitrarily choosing a large value of $r' = 1.1$ means that all neighboring particles within 10% of the reference particle diameter are in contact. This contact criterion significantly overestimates the contact number at ϕ_J by generating values of $\langle z \rangle_J \approx 8.0$ and $\langle z \rangle_J \approx 6.4$ for smooth and rough colloids respectively. Instead, we use the estimated contact criterion of $r' = 1.04$ for smooth colloids and find that $\langle z \rangle_J \approx 5.5$, much closer to the expected isostatic criterion ($z_{iso} = 6$) for frictionless spheres. Using $r' = 1.06$ causes a slight overestimation of the contact number at jamming, $\langle z \rangle_J \approx 6.3$. The limits of the contact criterion for the smooth colloids is therefore $1.04 < r' < 1.06$. Applying the same analysis to suspensions of rough colloids ($1.05 \leq r' \leq 1.07$) produces $4 \leq \langle z \rangle_J \leq 4.8$ and validates the choice of $r' = 1.05$ from the uncertainty analysis on cutoff distance.

Fig. 9 shows how p(z) varies with r' in suspensions of smooth ($r' = 1.04$ and 1.06) and rough ($r' = 1.05$ and 1.07) colloids. The difference in p(z) are relatively minor at small ϕ but becomes rather significant in dense suspensions with larger values of ϕ. As expected, the p(z) plots for smooth colloids show that increasing ϕ causes $\langle z \rangle$ to shift towards higher values while the spread remains relatively constant except at $\phi = 0.20$ (**Fig. 9a and 9c)**. The inset of these figures show that $\langle z \rangle$ increases from 0 to 6 as ϕ approaches 0.64. Similarly in the case of rough

colloids, $\langle z \rangle$ increases with increasing ϕ (**Fig. 9b and 9d**). At ϕ_J, changing the contact criterion for rough colloids increases $\langle z \rangle_J$ from 4 ($r' = 1.05$) to 4.9 ($r' = 1.07$). The exact isostatic condition of the particle depends on its μ_p.

The sensitivity of $\langle z \rangle_J$ to r' is shown in **Fig. 10.** Both smooth and rough colloids show a linear relation of $\langle z \rangle_J$ to r' with a small slope. As r' increases from 1.04 to 1.06 for smooth colloids, $\langle z \rangle_J$ increases from 5.5 ± 0.7 to 6.3 ± 0.7. Similarly, as r' increases from 1.05 to 1.07 for rough colloids, $\langle z \rangle_J$ increases from 4.0 ± 0.9 to 4.9 ± 0.9. The uncertainty in $\langle z \rangle_J$ values shown in **Fig. 10** are not from experimental errors but are from the error propagation estimated in the nonlinear fits that were used to extrapolate $\langle z \rangle$ at various ϕ to the shear jammed states. The contact criterion of $r' = 1.04$ as established by our method shows that $\langle z \rangle_J \approx 6$ for smooth colloids to within error limits. It is possible to further narrow down the contact criterion to $r' = 1.052$, where $\langle z \rangle_J = 6 \pm 0.7$, pointing to the contact criterion that is applicable to the ideal isostatic condition, where $\phi_J \approx \phi_{RCP}$ and $\langle z \rangle_J \approx z_{iso}$. Furthermore, without the need to explicitly measure surface roughness or interparticle friction, the method shows that $4.0 \leq \langle z \rangle_J \leq 4.9$ in the contact search window $1.05 \leq r' \leq 1.07$ for the rough colloids. Various literature studies involving theory and simulations predict a similar window of contact where $4 < z_{RCP} < 4.5$ for frictional particles at $\phi_J = 0.56$[12, 81-83] in support of the validity our contact criterion within the error limits. Compared to smooth colloids, we are unable to narrow down a single value of the contact distance for which we require prior knowledge of isostatic condition of the particle, which in turn depends on its μ_p. Nonetheless, we have provided a window of the contact criterion for rough hard sphere colloids where the mean number of particle-particle contacts at jamming is within error limits as predicted by theory and simulations.

4. Conclusions

The sensitivity analyses in **Fig. 8, 9, and 10** demonstrate that a physically relevant search distance is needed to quantify the contact microstructure of dense colloidal suspensions. Picking a value of r' that deviates by just 1% of the particle diameter results in a change in $\langle z \rangle$ by up to 10% of the true value. This effect is exacerbated in dense suspensions ($\phi > 0.50$) because of the increased number of nearest neighbors around a reference centroid. In fact, our results show that the conventional practice of using the first minimum in $g(r)$ is inappropriate because using such a large search distance drastically overestimates $\langle z \rangle$. Rather, we recommend performing a simple uncertainty analysis that accounts for the size polydispersity, steric brush length, and surface roughness of the colloids. Summing the physical length scales with the swollen particle radius generates a search criterion which varies between $r' = 1.04$ and $r' = 1.07$ for both smooth and rough colloids. To prepare the samples in this paper, sterically stabilized PHSA-g-PMMA colloids are packed to ϕ_J using a shear jamming protocol in a high speed centrifuge at Pe >> 1, which avoids crystallization of the monodisperse particles over experimental time scales while shifting ϕ_J to values below ϕ_{RCP}.

The method we developed here can be used to find an appropriate contact search distance for spherically-symmetric particles with surface roughness, without requiring prior knowledge of ϕ_{RCP} and μ_p. History-dependent effects could be important when approaching or departing from the shear jammed point, especially for frictional particles. The established procedure could potentially be extrapolated to other types of particulate systems where electrostatic interactions play a role, or in predicting the jamming threshold for biological systems and geological soils.[84, 85]

Conflicts of Interest

The authors declare no conflicts of interest.

Acknowledgements

The authors thank Dr. Alan Jacob, Prof. Karen Daniels, and Prof. Eric Weeks for advice and discussion. We acknowledge the Analytical Instrumentation Facility (AIF) at NC State University for SEM and AFM facilities. This work is supported in part by the National Science Foundation (NSF CBET-1804462), the American Chemical Society Petroleum Research Fund (#59208-DNI9), and North Carolina State University startup funds.

References

1. J. J. Stickel and R. L. Powell, *Annual Review of Fluid Mechanics*, 2005, **37**, 129-149.
2. M. van Hecke, *Journal of Physics: Condensed Matter*, 2009, **22**, 033101.
3. J.-A. Park, J. H. Kim, D. Bi, J. A. Mitchel, N. T. Qazvini, K. Tantisira, C. Y. Park, M. McGill, S.-H. Kim, B. Gweon, J. Notbohm, R. Steward, Jr., S. Burger, S. H. Randell, A. T. Kho, D. T. Tambe, C. Hardin, S. A. Shore, E. Israel, D. A. Weitz, D. J. Tschumperlin, E. P. Henske, S. T. Weiss, M. L. Manning, J. P. Butler, J. M. Drazen and J. J. Fredberg, *Nat Mater*, 2015, **14**, 1040-1048.
4. J. M. Pastor, A. Garcimartín, P. A. Gago, J. P. Peralta, C. Martín-Gómez, L. M. Ferrer, D. Maza, D. R. Parisi, L. A. Pugnaloni and I. Zuriguel, *Phys Rev E*, 2015, **92**, 062817.
5. I. Zuriguel, A. Garcimartín, D. Maza, L. A. Pugnaloni and J. M. Pastor, *Phys Rev E*, 2005, **71**, 051303.
6. A. J. Liu and S. R. Nagel, *Nature*, 1998, **396**, 21-22.
7. C. S. O'Hern, L. E. Silbert, A. J. Liu and S. R. Nagel, *Phys Rev E*, 2003, **68**, 011306.
8. M. E. Cates, J. P. Wittmer, J. P. Bouchaud and P. Claudin, *Phys Rev Lett*, 1998, **81**, 1841-1844.
9. T. S. Majmudar and R. P. Behringer, *Nature*, 2005, **435**, 1079-1082.
10. S. Henkes and B. Chakraborty, *Phys Rev E*, 2009, **79**, 061301.
11. J. E. Thomas, K. Ramola, A. Singh, R. Mari, J. F. Morris and B. Chakraborty, *Phys Rev Lett*, 2018, **121**, 128002.
12. R. Radhakrishnan, J. R. Royer, W. C. K. Poon and J. Sun, *Granular Matter*, 2020, **22**, 29.
13. K. A. Whitaker, Z. Varga, L. C. Hsiao, M. J. Solomon, J. W. Swan and E. M. Furst, *Nature Communications*, 2019, **10**, 2237.
14. R. N. Zia, B. J. Landrum and W. B. Russel, *Journal of Rheology*, 2014, **58**, 1121-1157.
15. S. Jamali, G. H. McKinley and R. C. Armstrong, *Phys Rev Lett*, 2017, **118**, 048003.
16. A. Zaccone, H. Wu and E. Del Gado, *Phys Rev Lett*, 2009, **103**, 208301.
17. L. C. Hsiao, H. Kang, K. H. Ahn and M. J. Solomon, *Soft Matter*, 2014, **10**, 9254-9259.
18. E. Moghimi, A. R. Jacob and G. Petekidis, *Soft Matter*, 2017, **13**, 7824-7833.
19. W. G. Ellenbroek, M. van Hecke and W. van Saarloos, *Phys Rev E*, 2009, **80**, 061307.
20. E. Somfai, M. van Hecke, W. G. Ellenbroek, K. Shundyak and W. van Saarloos, *Phys Rev E*, 2007, **75**, 020301.
21. M. Otsuki and H. Hayakawa, *Phys Rev E*, 2017, **95**, 062902.
22. F. Scheffold, F. Cardinaux and T. G. Mason, *Journal of Physics: Condensed Matter*, 2013, **25**, 502101.
23. A. Donev, I. Cisse, D. Sachs, E. A. Variano, F. H. Stillinger, R. Connelly, S. Torquato and P. M. Chaikin, *Science*, 2004, **303**, 990-993.
24. A. Baule and H. A. Makse, *Soft Matter*, 2014, **10**, 4423-4429.
25. A. Boromand, A. Signoriello, F. Ye, C. S. O'Hern and M. D. Shattuck, *Phys Rev Lett*, 2018, **121**, 248003.
26. M. Clusel, E. I. Corwin, A. O. N. Siemens and J. Brujić, *Nature*, 2009, **460**, 611-615.
27. C. Zhang, C. B. O'Donovan, E. I. Corwin, F. Cardinaux, T. G. Mason, M. E. Möbius and F. Scheffold, *Physical Review E*, 2015, **91**, 032302.
28. T. G. Mason, J. Bibette and D. A. Weitz, *Physical Review Letters*, 1995, **75**, 2051-2054.
29. T. G. Mason, M.-D. Lacasse, G. S. Grest, D. Levine, J. Bibette and D. A. Weitz, *Physical Review E*, 1997, **56**, 3150-3166.
30. J. Mewis and N. J. Wagner, *Colloidal Suspension Rheology*, Cambridge University Press, Cambridge, 2011.
31. J. F. Brady, *Journal of Fluid Mechanics*, 1994, **272**, 109-134.
32. R. J. Phillips, J. F. Brady and G. Bossis, *The Physics of Fluids*, 1988, **31**, 3473-3479.

33. L. C. Hsiao and S. Pradeep, *Current Opinion in Colloid & Interface Science*, 2019, **43**, 94-112.
34. M. Jerkins, M. Schröter, H. L. Swinney, T. J. Senden, M. Saadatfar and T. Aste, *Physical Review Letters*, 2008, **101**, 018301.
35. R. A. Lionberger and W. B. Russel, *Journal of Rheology*, 1994, **38**, 1885-1908.
36. T. Shikata and D. S. Pearson, *Journal of Rheology*, 1994, **38**, 601-616.
37. J. F. Brady, *The Journal of Chemical Physics*, 1993, **99**, 567-581.
38. B. M. Guy, M. Hermes and W. C. K. Poon, *Physical Review Letters*, 2015, **115**, 088304.
39. C. P. Hsu, S. N. Ramakrishna, M. Zanini, N. D. Spencer and L. Isa, *P Natl Acad Sci USA*, 2018, **115**, 5117-5122.
40. L. C. Hsiao, I. Saha-Dalal, R. G. Larson and M. J. Solomon, *Soft Matter*, 2017, **13**, 9229-9236.
41. B. Schroyen, C.-P. Hsu, L. Isa, P. Van Puyvelde and J. Vermant, *Phys Rev Lett*, 2019, **122**, 218001.
42. G. M. Conley, P. Aebischer, S. Nöjd, P. Schurtenberger and F. Scheffold, *Science Advances*, 2017, **3**, e1700969.
43. L. Mohan, R. T. Bonnecaze and M. Cloitre, *Phys Rev Lett*, 2013, **111**, 268301.
44. Z. Zhou, J. V. Hollingsworth, S. Hong, H. Cheng and C. C. Han, *Langmuir*, 2014, **30**, 5739-5746.
45. D. Vlassopoulos and M. Cloitre, *Current Opinion in Colloid & Interface Science*, 2014, **19**, 561-574.
46. C. J. Dibble, M. Kogan and M. J. Solomon, *Phys Rev E*, 2006, **74**.
47. P. G. De Gennes, *J. Physique Lett.*, 1976, **37**, 1-2.
48. M. C. Jenkins, M. D. Haw, G. C. Barker, W. C. K. Poon and S. U. Egelhaaf, *Soft Matter*, 2011, **7**, 684-690.
49. M. C. Jenkins, M. D. Haw, G. C. Barker, W. C. K. Poon and S. U. Egelhaaf, *Phys Rev Lett*, 2011, **107**.
50. J. D. Bernal and J. Mason, *Nature*, 1960, **188**, 910-911.
51. J. Brujić, C. Song, P. Wang, C. Briscoe, G. Marty and H. A. Makse, *Physical Review Letters*, 2007, **98**, 248001.
52. L. Antl, J. W. Goodwin, R. D. Hill, R. H. Ottewill, S. M. Owens, S. Papworth and J. A. Waters, *Colloid Surface*, 1986, **17**, 67-78.
53. L. Palangetic, K. Feldman, R. Schaller, R. Kalt, W. R. Caseri and J. Vermant, *Faraday Discuss*, 2016, **191**, 325-349.
54. L. E. Silbert, *Soft Matter*, 2010, **6**, 2918-2924.
55. B. A. D. Costello, P. F. Luckham and T. F. Tadros, *Langmuir*, 1992, **8**, 464-468.
56. P. N. Pusey and W. Vanmegen, *Nature*, 1986, **320**, 340-342.
57. N. M. James, H. Xue, M. Goyal and H. M. Jaeger, *Soft Matter*, 2019, **15**, 3649-3654.
58. I. R. Peters, S. Majumdar and H. M. Jaeger, *Nature*, 2016, **532**, 214-217.
59. D. Bi, J. Zhang, B. Chakraborty and R. P. Behringer, *Nature*, 2011, **480**, 355-358.
60. G. L. Hunter and E. R. Weeks, *Reports on Progress in Physics*, 2012, **75**, 066501.
61. J. C. Crocker and D. G. Grier, *J Colloid Interf Sci*, 1996, **179**, 298-310.
62. R. S. Farr and R. D. Groot, *The Journal of Chemical Physics*, 2009, **131**, 244104.
63. S.-E. Phan, W. B. Russel, J. Zhu and P. M. Chaikin, *The Journal of Chemical Physics*, 1998, **108**, 9789-9795.
64. W. Schaertl and H. Sillescu, *Journal of Statistical Physics*, 1994, **77**, 1007-1025.
65. K. W. Desmond and E. R. Weeks, *Physical Review E*, 2014, **90**, 022204.
66. R. P. A. Dullens, *Soft Matter*, 2006, **2**, 805-810.
67. W. C. K. Poon, E. R. Weeks and C. P. Royall, *Soft Matter*, 2012, **8**, 21-30.
68. L. S. Ornstein and F. Zernike, *P K Akad Wet-Amsterd*, 1914, **17**, 793-806.
69. J. K. Percus and G. J. Yevick, *Phys Rev*, 1958, **110**, 1-13.
70. P. Varadan and M. J. Solomon, *Langmuir*, 2003, **19**, 509-512.

71. C. Zhang, N. Gnan, T. G. Mason, E. Zaccarelli and F. Scheffold, *Journal of Statistical Mechanics: Theory and Experiment*, 2016, **2016**, 094003.
72. L. C. Hsiao, R. S. Newman, S. C. Glotzer and M. J. Solomon, *P Natl Acad Sci USA*, 2012, **109**, 16029-16034.
73. L. C. Hsiao, M. J. Solomon, K. A. Whitaker and E. M. Furst, *Journal of Rheology*, 2014, **58**, 1485-1504.
74. P. Varadan and M. J. Solomon, *Journal of Rheology*, 2003, **47**, 943-968.
75. A. I. Campbell, V. J. Anderson, J. S. van Duijneveldt and P. Bartlett, *Phys Rev Lett*, 2005, **94**, 208301.
76. J.-P. Hansen and I. R. McDonald, *Theory of Simple Liquids*, Academic Press, Oxford, 2013.
77. A. Doroszkowski and R. Lambourne, *Journal of Colloid and Interface Science*, 1968, **26**, 214-221.
78. R. J. R. Cainrs, R. H. Ottewill, D. W. J. Osmond and I. Wagstraff, *Journal of Colloid and Interface Science*, 1976, **54**, 45-51.
79. G. Bryant, S. R. Williams, L. Qian, I. K. Snook, E. Perez and F. Pincet, *Physical Review E*, 2002, **66**, 060501.
80. L. C. Hsiao, S. Jamali, E. Glynos, P. F. Green, R. G. Larson and M. J. Solomon, *Phys Rev Lett*, 2017, **119**.
81. J. I. N. Sun and S. Sundaresan, *Journal of Fluid Mechanics*, 2011, **682**, 590-616.
82. H. A. Vinutha and S. Sastry, *Nature Physics*, 2016, **12**, 578-583.
83. C. Song, P. Wang and H. A. Makse, *Nature*, 2008, **453**, 629-632.
84. M. Delarue, J. Hartung, C. Schreck, P. Gniewek, L. Hu, S. Herminghaus and O. Hallatschek, *Nature Physics*, 2016, **12**, 762.
85. B. Ferdowsi, C. P. Ortiz and D. J. Jerolmack, *P Natl Acad Sci USA*, 2018, **115**, 4827-4832.

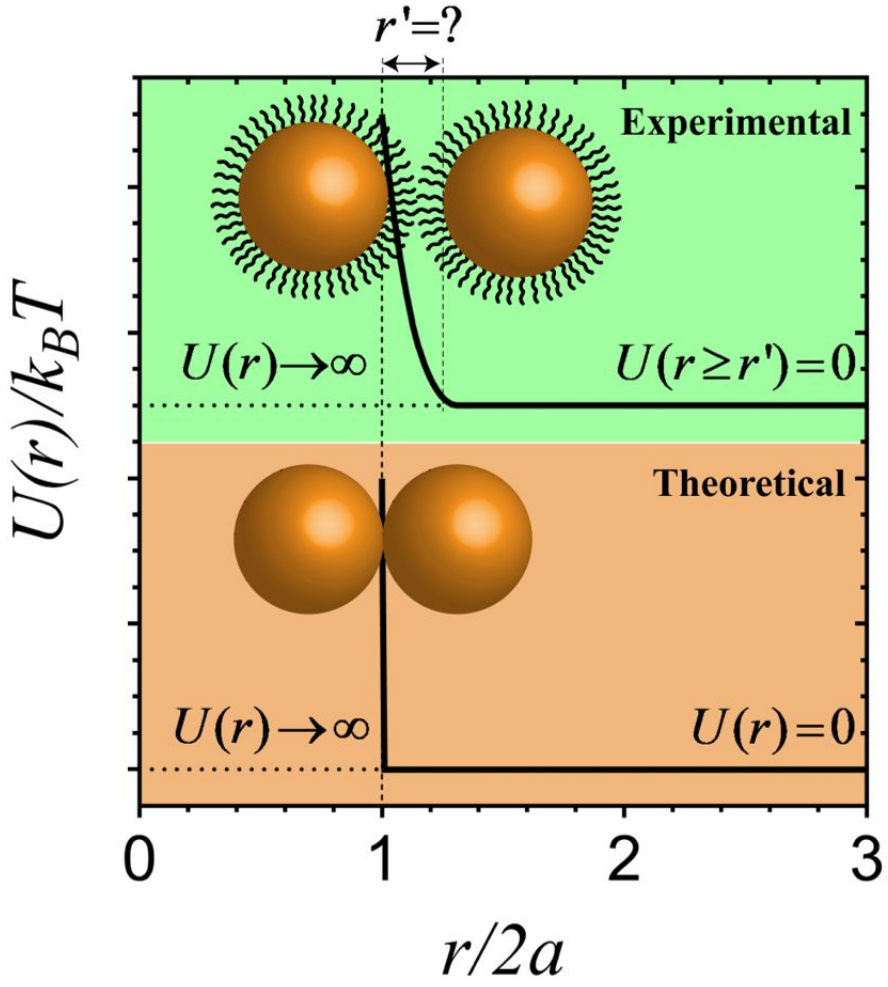

Fig. 1 Difference in the pairwise interaction potential between theoretical and experimental hard-sphere systems. The experimental system consists of poly(methyl methacrylate) colloids sterically stabilized with a thin layer of poly(12-hydroxystearic acid).

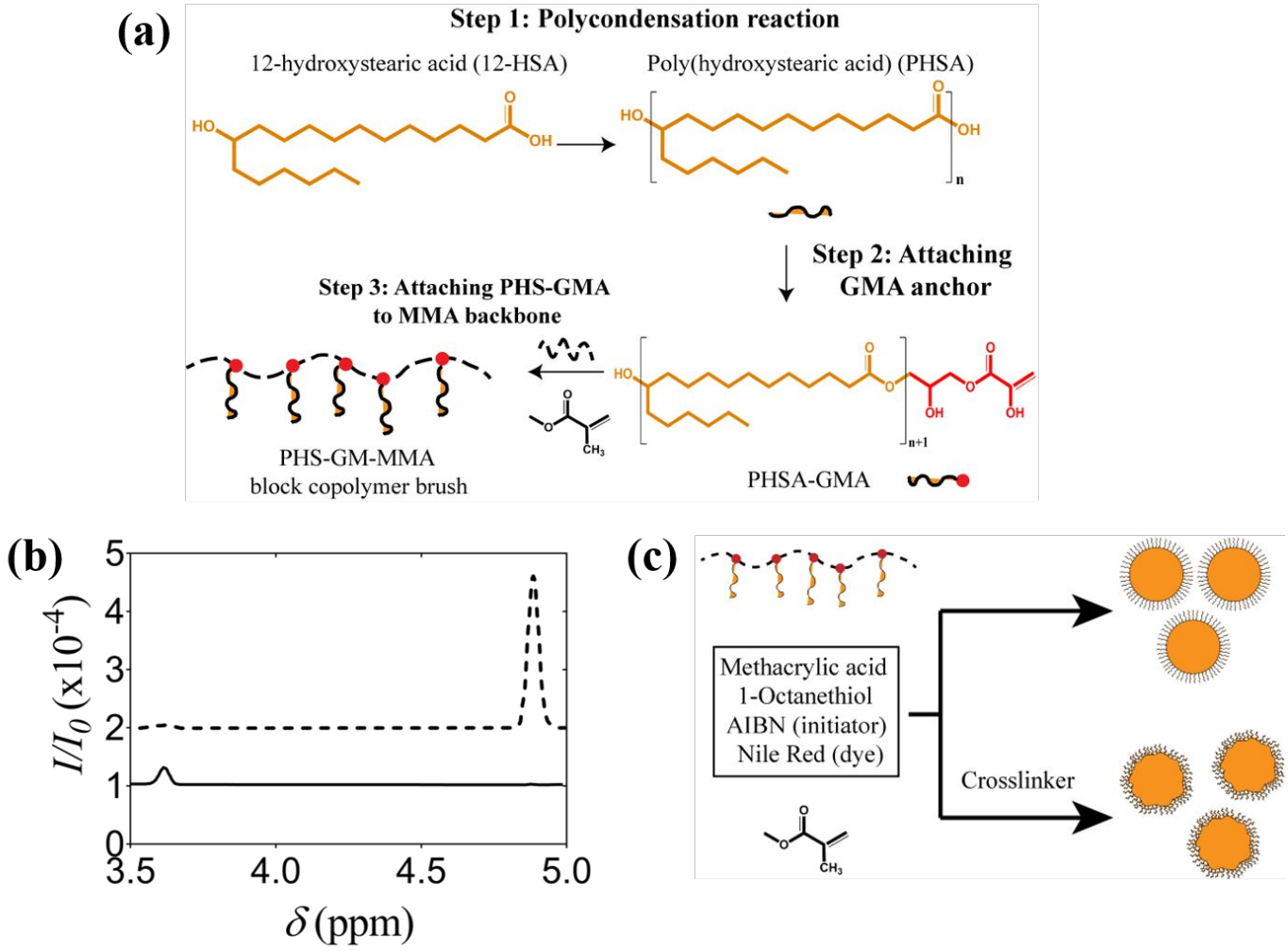

Fig. 2 (a) Chemical reaction scheme for the PHSA stabilizer. (b) ^{1}H-NMR spectra for 12-HSA (bold line) and PHS-GMA (dashed line) with chemical shift as a function of normalized intensity with respect to the reference standard, d-$CHCl_3$. (c) Overview of the synthesis protocol for PHSA-g-PMMA smooth and rough colloids.

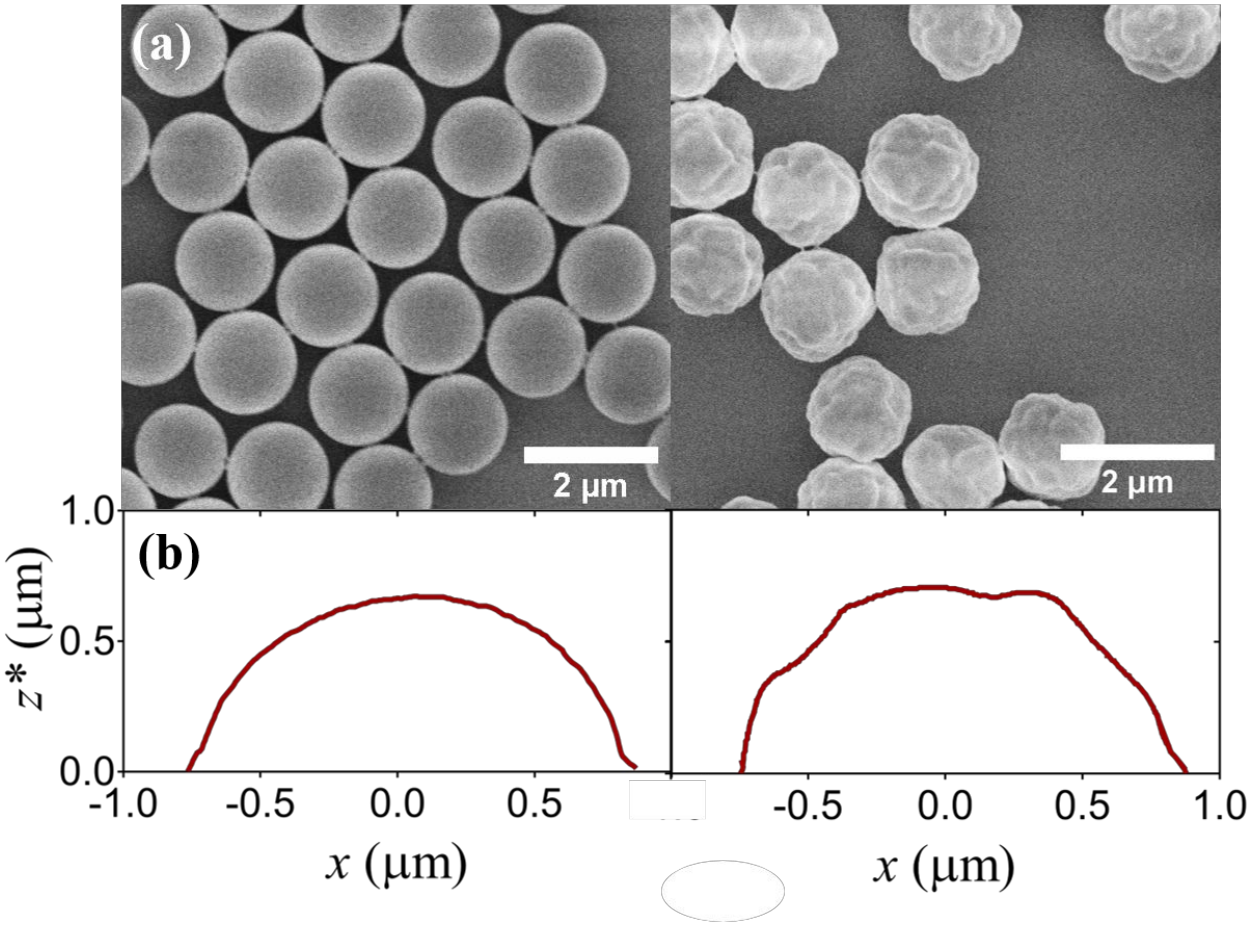

Fig. 3 Characterization of the colloid morphology. (a) SEM micrographs and (b) 2D AFM surface profiles for smooth (left) and rough (right) colloids. The profiles are taken at close to the center plane of the colloids. In (b), z^* refers to regions that are not limited by the AFM cantilever geometry.

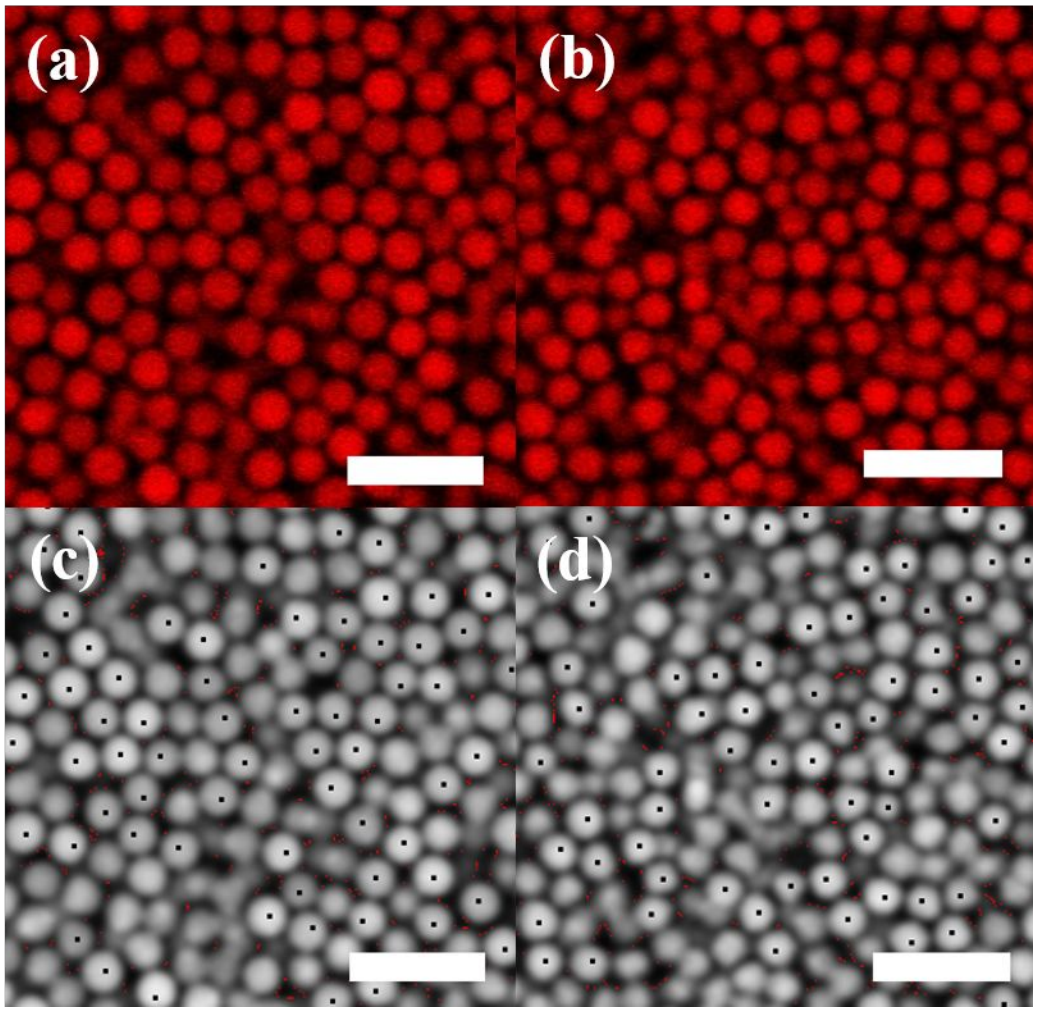

Fig. 4 (a,b) Representative raw CLSM images and (c,d) processed images where black dots indicate centroid positions in a fixed plane. (a, c) Dense suspension of smooth colloids at ϕ = 0.61, (b, d) dense suspension of rough colloids at ϕ = 0.54. Scales bars = 5 μm.

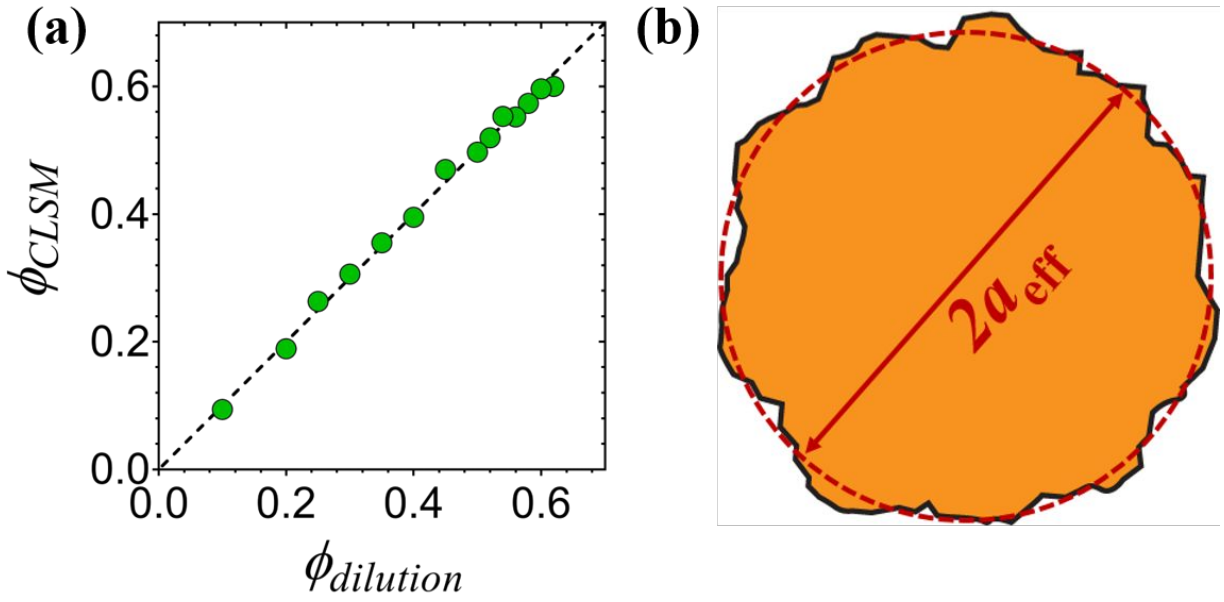

Fig. 5 (a) Comparison of the colloid volume fraction using two methods: high speed centrifugation to a shear jammed packing followed by subsequent dilutions, and directly counting number of particles from CLSM. (b) Method to extract the effective diameter and volume fraction of rough colloids.

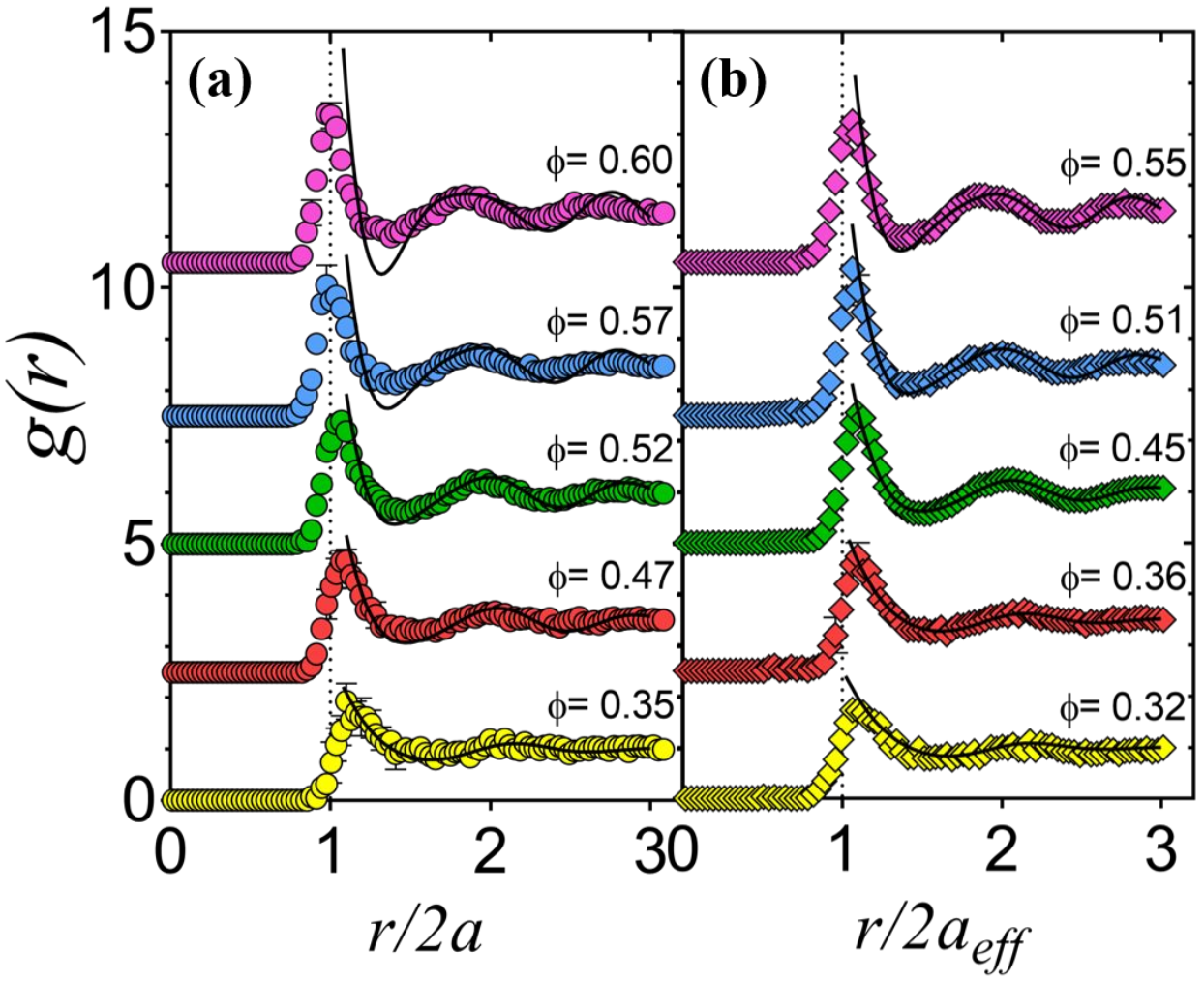

Fig. 6 Radial distribution functions of (a) smooth and (b) rough colloids. Filled circles represent experimental values and solid black lines represent the theoretical fits from the Ornstein-Zernicke solutions. In (a), the $g(r)$ data set are plotted for smooth colloids at $\phi = 0.35$ (yellow), $\phi = 0.47$ (red), $\phi = 0.52$ (green), $\phi = 0.57$ (blue), and $\phi = 0.60$ (pink). In (b), the $g(r)$ data set are plotted for rough colloids at $\phi = 0.32$ (yellow), $\phi = 0.36$ (red), $\phi = 0.45$ (blue), $\phi = 0.51$ (red), and $\phi = 0.55$ (pink).

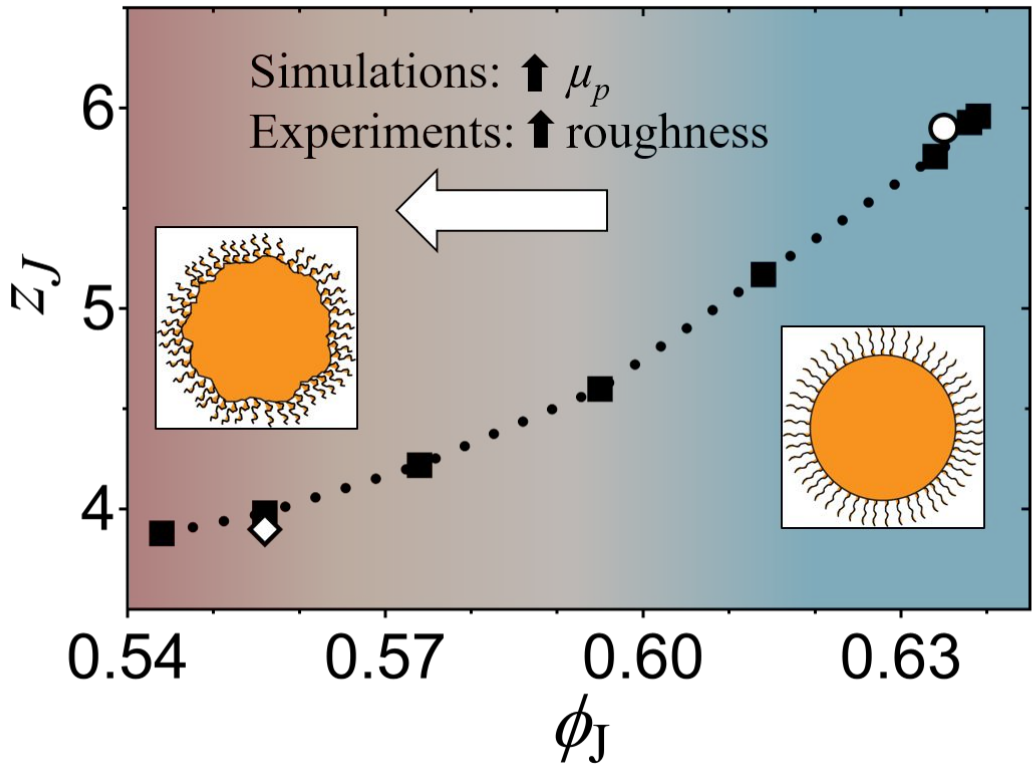

Fig. 7 The contact number at jamming plotted against the volume fraction at jamming, which is a function of the interparticle friction. Filled squares are data adapted from simulations of Silbert.[54] A dotted line is drawn to guide the eye. Open symbols represent experimental data for smooth (circle) and rough (diamond) colloids. The experimental z_J values are obtained by using $r' = 1.04$ for smooth colloids and $r' = 1.05$ for rough colloids. Color gradient indicates transition from frictionless (red) to infinite friction (blue) regime. Inset: Sketch of smooth and rough PMMA particles with PHSA brushes for illustration purposes.

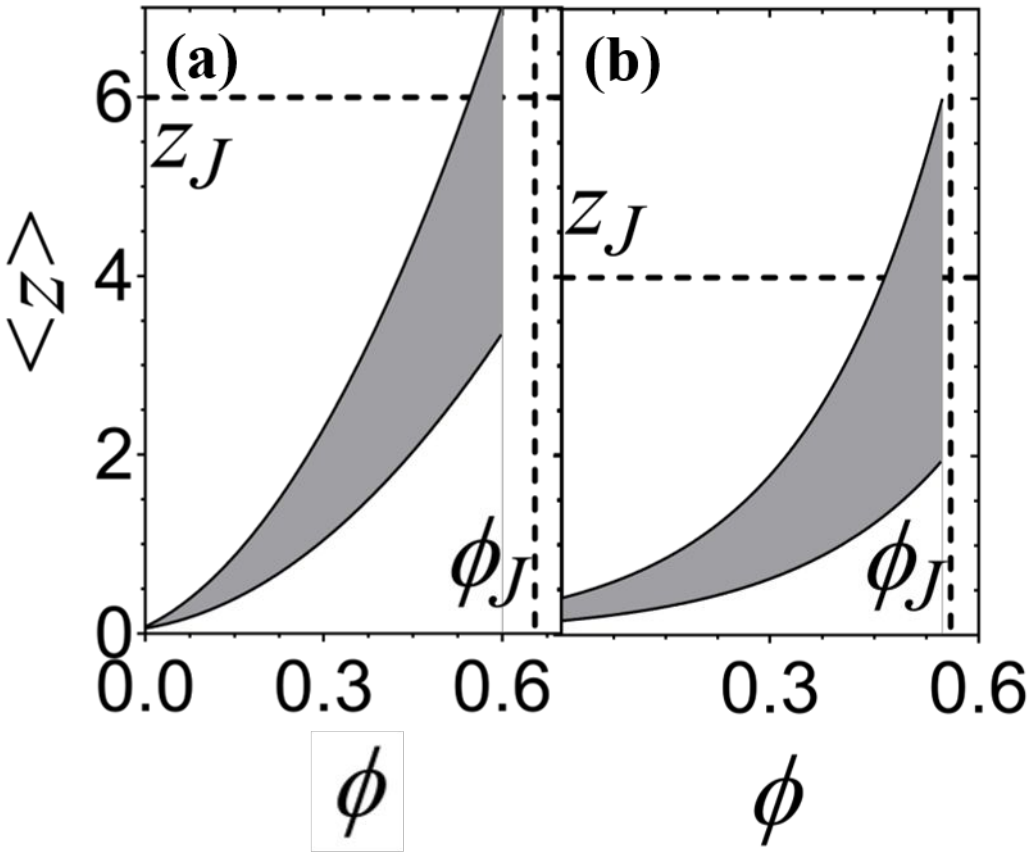

Fig. 8 Plot of the mean contact number as a function of ϕ for (a) smooth and (b) rough colloids. Shaded regions indicate a range of <z> values for different search distances used. The upper limit is for $r' = 1.1$ and the lower limit is for $r' = 1.0$. Dashed lines indicate predictions for isostatic packings of (a) frictionless and (b) frictional particles adapted from ref. 46. (Silbert, 2010).

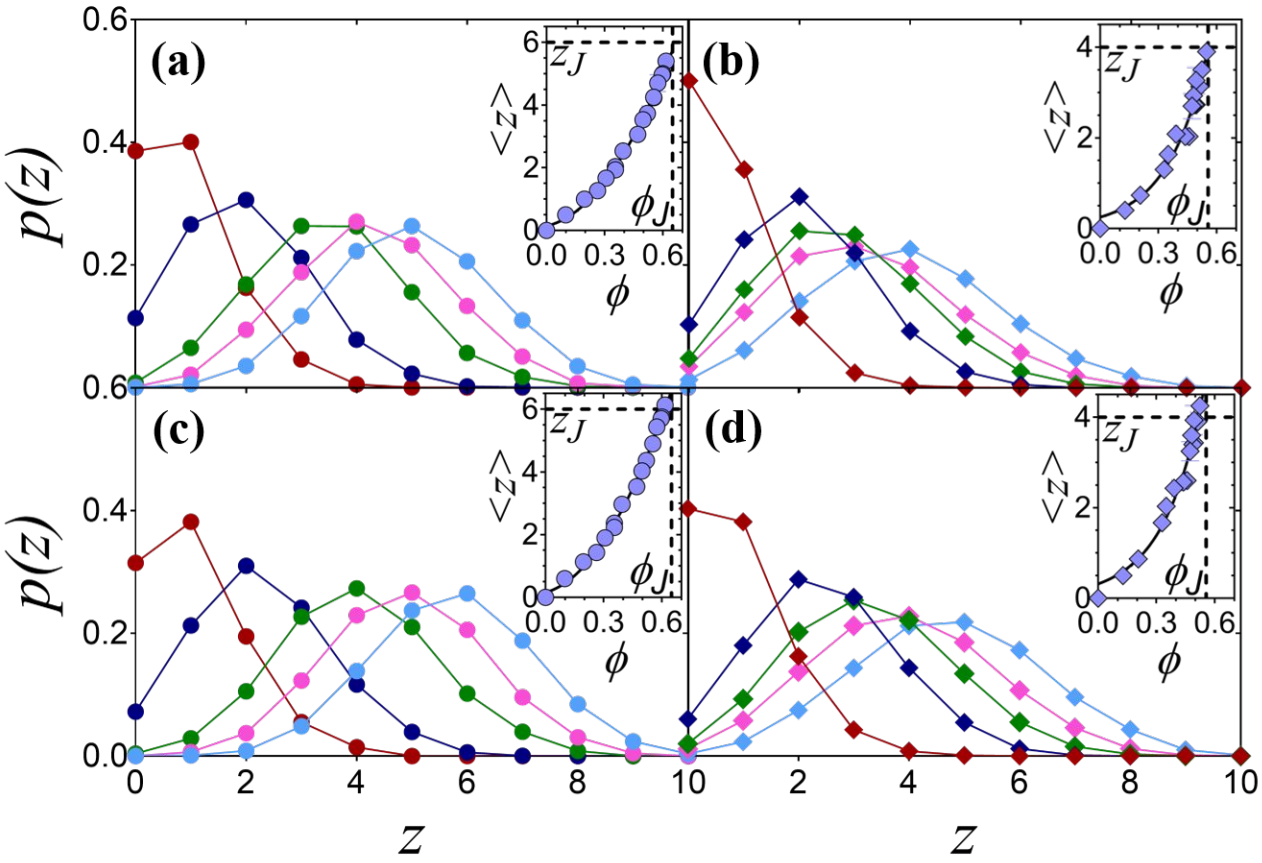

Fig. 9 (a, c) Contact number distributions for smooth colloids obtained by setting (a) $r' = 1.04$ and (c) $r' = 1.06$. (b, d) Contact number distributions for rough colloids obtained by setting (b) $r' = 1.05$ and (d) $r' = 1.07$. For smooth colloids, the data sets consist of suspensions at $\phi = 0.20$ (red), $\phi = 0.35$ (dark blue), $\phi = 0.50$ (green), $\phi = 0.55$ (pink), and $\phi = 0.60$ (aqua). For rough colloids, the data sets consist of suspensions at $\phi = 0.20$ (red), $\phi = 0.40$ (dark blue), $\phi = 0.47$ (green), $\phi = 0.52$ (pink), and $\phi = 0.55$ (aqua). Insets: Mean contact number of smooth colloids with (a) $r' = 1.04$ and (c) $r' = 1.06$ and rough colloids with (b) $r' = 1.05$ and (d) $r' = 1.07$.

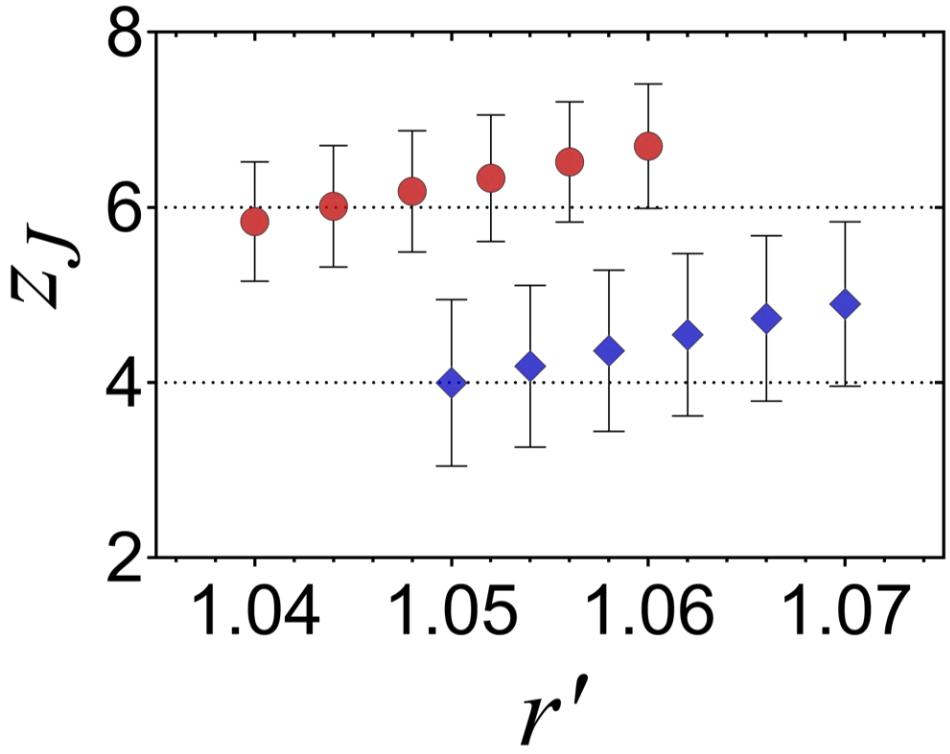

Fig. 10 Sensitivity analysis plot shows how z_J varies as a function of r' for smooth (red circles) and rough (blue diamonds) colloids at their respective extrapolated values of ϕ_J. Dotted lines represent isostatic conditions for frictionless ($z_J = 6$, $\mu_p = 0$) and frictional ($z_J = 4$, $\mu_p \rightarrow \infty$) particles.